# OPTICAL DEFORMATION POTENTIALS FOR PbSe AND PbTe

**I. I. Zasavitskii[1], E. A. de Andrada e Silva[2], E. Abramof[2], P. J. McCann[3]**

[1]*P. N. Lebedev Physical Institute of RAS, Leninskii Pr. 53, 119991 Moscow, Russia*

[2]*Insituto Nacional de Pesquisas Espaciais – INPE, CP515, 12201-970 Sao Jose dos Campos-SP, Brazil*

[3]*School of Electrical and Computer Engineering, University of Oklahoma, Norman, Oklahoma 73019*

The values of optical deformation potentials ($D_u$ and $D_d$) for PbSe and PbTe are analyzed using absorption, luminescence and X-ray diffraction data on high quality, deep quantum well PbSe/PbSrSe and PbTe/PbEuTe structures. It is important for these evaluations to use the value of isotropic deformation potential ($D_{iso}$) which is determined from the low temperature hydrostatic pressure experiments and the intervalley splitting which was determined from differential absorption spectroscopy. The fitting procedure was done using an accurate **k·p** model for the band structure near the fundamental gap including anisotropy, multi-valley, and band nonparabolicity effects. We find the new optical deformation potential values at 4 K: $D_u$ = - 0.2 and – 0.5 eV, and $D_d$ = 5.3 and 3.5 eV for PbSe and PbTe, respectively.

## 1. Introduction

There is a considerable interest to the energy spectrum changes due to strain in semiconductor multi-quantum well (MQW) heterostructures. It is especially important in the case of IV-VI semiconductors because good lattice matching is restricted to four-component solid solutions and in view of the lack of good substrates, particularly for PbSe. As a result, the most common IV-VI MQW structures are strained and, as optical experiments have shown, the elastic strains in this case result in noticeable spectral changes (up to 20 meV or ~ 10 % of the energy gap). Energy spectra depend on the strain and deformation potential values, which in their turn are not well known for the Pb salts. So far, the theoretically and experimentally determined deformation potentials are spread over a wide range. In Table I, we have listed the obtained theoretical values [1-3] together with those obtained experimentally [4-7] by different groups. The mentioned large variation is clearly seen and calls for both more calculations and measurements.

In particular, considerable discrepancies still remain among the data for the optical deformation potentials $D_d$ and $D_u$. With a few exceptions [6], most $D_d$ and $D_u$ values do not agree with the isotropic (volume) deformation potential $D_{iso} = 3\ D_d + D_u$, determined with good accuracy from hydrostatic pressure experiments at different temperatures [6,8]. On the other hand, previous optical studies of IV-VI strained structures [6,9] were based on the model that in these structures the lowest energy transition belongs to the normal (longitudinal) valley. Recent differential transmission spectroscopy of PbSe/PbSrSe/$BaF_2$(111) MQW structures clearly demonstrates this validity at well widths up to 30 nm [10]. An important aspect of this work is that the authors [10] were able to measure

the intervalley splitting which results directly in one ($D_u$) of deformation potential constants and the next one ($D_d$) can be obtained from the $D_{iso}$ relation.

Presented here is a detailed analysis of the absorption and PL spectra of high quality PbSe/PbSrSe and PbTe/PbEuTe MQW structures at different sample temperatures.

Table 1. Acoustic ($D_d^{c,v}$ and $D_u^{c,v}$) and optical ($D_d = D_d^c - D_d^v$ and $D_u = D_u^c - D_u^v$) deformation potential values for the IV-VI semiconductors (in eV)

| Material | $D_d^c$ | $D_u^c$ | $D_d^v$ | $D_u^v$ | $D_d$ | $D_u$ | $D_{iso}$ | References |
|---|---|---|---|---|---|---|---|---|
| PbSe | - 2.67 | 2.56 | - 9.15 | 4.67 | 6.48 | - 2.11 | 17.24 | Rabii [2] |
| | | 1.06 | | 3.14 | | - 2.08 | | Enders [3] |
| | | | | | 6.5 | - 3.7 | 15.8 | Valeiko [6] |
| | | | | | 6.1 | - 1.3 | 17.0 | Wu [7] |
| | | | | | 5.3 | -0.2 | 15.7 | 4 K |
| | | | | | 5.33 | -0.6 | 15.4 | 77 K } this work |
| | | | | | 4.9 | -0.7 | 14.0 | 300 K |
| PbTe | - 4.36 | 8.29 | -8.93 | 10.46 | 4.57 | - 2.17 | 11.55 | Ferreira [1] |
| | | 0.297 | | 2.48 | | - 2.18 | | Enders [3] |
| | - 1.09 | 2.07 | - 2.23 | 2.62 | 1.14 | - 0.55 | 2.87 | Kriechbaum [4] |
| | | | 4.9 | 5.4 | 1.9 | - 0.5 | 6 (5.2) | Singleton [5] |
| | | | | | 4.3 | - 2.8 | 10.1 | Valeiko [6] |
| | | ± 0.5 | | 1 | 3.53 | - 0.5 | 10.1 | ~ 4 K, this work |

Published data for PbTe/$BaF_2$ strained structures were also used. Based on the experimentally determined $D_{iso}$ and the unambiguously determined well-width dependent intervalley splitting we have used a fitting procedure within an accurate two-band **k·p** model for the low energy transitions. This permitted the determination of new values for the PbSe and PbTe optical deformation potentials, which fit best the available data.

## 2.Theory

For the present purpose, the deformation potential can be simply defined with the general expression for the band-edge energy shift due to strain, i.e.:

$$\delta E_{c,v} = \sum_{ij} D_{ij}^{c,v} \varepsilon_{ij} \,, \qquad (1)$$

where $D^{c,v}$ is the conduction or valence band deformation potential tensor and $\varepsilon$ is the strain tensor. The lead-salt band edge states at each of the four equivalent L points, except for Kramers degeneracy which is not removed with strain, are non-degenerate and, in the linear regime Eq. (1) is always valid. For these states, by cubic crystal symmetry, it is known that the deformation potential tensor is determined by only two independent constants, $D_d^{c,v}$ and $D_u^{c,v}$, the dilatation and uniaxial acoustic deformation potentials, respectively.

As given by Eq. (1), the strain energy shift depends on both deformation potential and strain tensors. If we consider only thin (under critical thickness) layers, i.e. pseudomorphic growth, we can assume homogeneous strain determined by the in-plane isotropic strain parameter

$$\varepsilon_{\|} = \frac{a_{\|}}{a} - 1, \tag{2}$$

where $a$ is the substrate material lattice constant and $a_{||}$ is the common in-plane lattice constant of the epitaxial layer or MQW structure, which can be measured with good accuracy in a high resolution X-ray diffractometer. The only other strain component is the out-of-the-plane or perpendicular strain that is proportional to the in-plane strain, i.e.

$$\varepsilon_{\perp} = -2\frac{C_{11} + 2C_{12} - 2C_{44}}{C_{11} + 2C_{12} + 4C_{44}}\varepsilon_{\|}, \tag{3}$$

with the proportionality constant given by the material elastic constants $C_{ij}$, which are known at different temperatures.

The energy shift due to uniaxial strain in IV-VI semiconductors is different for the gap states at L points orientated differently with respect to the strain axis; and, therefore, the valley degeneracy of these materials can be lifted by uniaxial strain. In addition, the populations of different valleys may also be different. In optical experiments with uniaxially strained samples both the energy shift and the valley splitting are observable.

Let's consider in detail the typical and important examples of uniaxial strain due to lattice mismatch in epitaxial layers or MQW structures grown along the [111] or [100] crystallographic directions, as defined by common substrates for the growth of IV-VI materials. The different valleys in case of [111] direction are divided into one orientated normally to the (111) plane in reciprocal space (i.e. along the [111] growth direction) and three equivalent ones along directions forming the same angle with the growth direction, which are called oblique valleys. The interband optical transition energies probed in absorption and PL experiments depend only on the strain induced energy shift of the fundamental band gap $E_g$ (and not on the valence and conduction band edge shifts independently). It is then convenient to define optical deformation potentials $D_d = D_d^c - D_d^v$ and $D_u = D_u^c - D_u^v$, so that the valley dependent energy gap strain shift is given by [5,9]

$$\delta E_g^N = D_d(2\varepsilon_{\|} + \varepsilon_{\perp}) + D_u\varepsilon_{\perp} \tag{4}$$

and

$$\delta E_g^O = D_d(2\varepsilon_{\|} + \varepsilon_{\perp}) + D_u(8\varepsilon_{\|} + \varepsilon_{\perp})/9, \tag{5}$$

for the normal and oblique valleys, respectively. In equations (4) and (5) the first term contributes to a shift in both the normal and oblique valleys by the same amount, while the second term contributes to a splitting of the two different valleys. The amount of this splitting depends only on the uniaxial deformation potential constant as follows:

$$\Delta = \delta E_g^{\ N} - \delta E_g^O = \frac{8}{9}D_u(\varepsilon_{\perp} - \varepsilon_{\|}). \tag{6}$$

In the case of [100]-oriented substrates all four valleys are equivalent, i.e. all the major axes of the ellipsoids make the same angle with the surface normal. The gap change is given by

$$\delta E_g^{[100]} = \frac{2(C_{11} - C_{12})}{3C_{11}}D_{iso}\varepsilon_{II}. \tag{7}$$

Here the isotropic (volume) deformation potential $D_{iso}$ is expressed through the optical deformation potentials as follows

$$D_{iso} = 3D_d + D_u = -(C_{11} + 2C_{12})\frac{dE_g}{dP}, \tag{8}$$

where $dE_g/dP$ is the volume hydrostatic pressure gap coefficient. For PbSe and PbTe, $D_{iso}$ has been measured with good accuracy at room and low temperatures. The $D_{iso}$ values are presented in Table 2.

Table 2. Elastic constants, hydrostatic pressure gap coefficients and $D_{iso}$ values

| Material | PbSe | | | PbTe | | |
|---|---|---|---|---|---|---|
| T, K | 4 | 77 | 298 | 4 | 77 | 303 |
| $C_{11}$ [a], $10^{10}$ N/m$^2$ | 14.18 | 13.98 | 12.37 | 12.81 | 12.43 | 10.80 |
| $C_{12}$ [a], $10^{10}$ N/m$^2$ | 1.94 | 1.97 | 1.93 | 0.44 | 0.47 | 0.77 |
| $C_{44}$ [a], $10^{10}$ N/m$^2$ | 1.749 | 1.695 | 1.591 | 1.514 | 1.482 | 1.344 |
| $(C_{11}+2C_{12})$[a], $10^{10}$ N/m$^2$ | 18.06 | 17.92 | 16.23 | 13.66 | 13.41 | 12.34 |
| $dE_g/dP$[b], $10^{-6}$ eV/bar | -8.7±0.8 | -8.6±0.2 | -8.6±0.1 | -7.4±0.8 | -7.4±0.2 | - 7.5 |
| $D_{iso}$, eV | 15.7 | 15.4 | 14.0 | 10.1 | 9.9 | 9.3 |

[a] Elastic constants were taken from Ref. 11 and Ref. 12 for PbTe and PbSe, respectively.
[b] The pressure gap coefficients at 4, 77 and 300 K see in [6,8].

In MQW structures, the optical transition energies include also the addition of both electron and hole quantum size (or confinement) shifts, $E_e$ and $E_h$, which besides being strongly well width dependent, can be calculated with high accuracy, especially for the lowest states, within the envelope function method based on a multi-band **k·p** model for the bulk (with the band gap and the electron band edge effective mass, both eventually strain shifted, as the only parameters). Therefore, if the strain is known, the optical deformation potentials remain the only two unknown parameters in the evaluation of the quantum well optical transition energies.

Due to the strong well width dependence of quantum size energies and due to the intervalley splitting sign dependence, several different energy level structures can occur. When the quantum size shift is zero or small, as in thick epitaxial layers or wide quantum well structures, the strain induced valley splitting is accurately approximated by equation (6), i.e. depends only on $D_u$. In PbTe/PbEuTe and PbSe/PbSrSe MQW structures, the active quantum well PbTe and PbSe layers present in-plane tensile strain, i.e. $a_{||} > a$ and $\varepsilon_{||}$ is positive. From Equations (3) and (6) it follows that if $D_u < 0$ $\Delta$ is, in this case, positive, meaning that the lowest optical transition in such an epitaxial layer or wide quantum well is from the oblique valleys. As the well width is reduced the confinement shifts for the oblique states increase much faster than that for the normal one (due to the much smaller oblique valley electron and hole effective mass along the growth direction); and, as a result, below a certain critical (crossing) well width the lowest transition is from the normal valley. Note that for $D_u > 0$, $|\Delta|$ increases monotonically with decreasing well width, and there is no crossing.

A two-band model accounting for band nonparabolicity, many-valley, and anisotropy effects is treated within the standard envelope function approximation [13]. Since PL intensity for both MQW structures was high, comparable with one of the best thick (2 – 3 μm) epilayers grown on $BaF_2$ substrates, the heterojunction is of type-I. There is no information about band offsets for these heterojunctions. Considering the mirror like band structure of these materials and the good agreement obtained with the measured absorption spectra (including the 3 nm QW sample) [9], we have used $\Delta E_c = \Delta E_v$ for our deep quantum wells ($\Delta E_g \geq 0.3$ eV at low temperatures), and checked that the lowest optical transition energies depend very little on deviations from such band edge discontinuities. Strain effects were also

included with the energy gap and the effective masses renormalization in accordance with previous considerations and the two-band model, respectively.

## 3. Strain

There are two strain sources in IV-VI MQW structures grown on $BaF_2$ substrates. The first one is the lattice mismatch between structural constituents, i.e. between well and barrier. The structure growth is usually started on a relatively thick (i.e. relaxed) buffer layer and the well and barrier layers are thinner than the critical layer thickness, so in the first approximation they are elastically and uniformly strained. Since the lattice constants of PbEuTe and PbSrSe solid solutions (barriers) are larger than PbTe and PbSe (wells), respectively, the wells are under tensile in-plane strain and the barriers under compressive in-plane strain. However, as the number of repetitions in our MQW samples is high (40 to 50), the MQW stack does not remain pseudomorphic (same in-plane lattice constant) to the buffer layer. It starts to relax and tends to a free-standing condition. This fact becomes especially important as the well width increases. It was demonstrated for PbTe quantum wells [14], where it was possible to fit the measured X-ray spectra of PbTe/PbEuTe MQW samples assuming a common in-plane lattice constant (different from the buffer value) for the whole MQW stack, and to determine the average strain in the PbTe wells. The fraction of the maximum parallel strain in the PbTe well decreased with the well width (by 26% at $L_z$ = 20 nm, see Figure 5 in Ref. 14).

Similar strain analysis was done here for PbSe quantum wells. The ω/2θ scan around the (222) Bragg diffraction peak was measured for the PbSe/PbSrSe MQW samples. In X-ray spectra there are the zero-order (most intense) plus several satellite peaks belonging to the MQW structure together with the $BaF_2$ substrate peak, which is used as a reference for the - axis. The PbSrSe buffer layer peak is overlapped by the zero-order peak for the sample with narrow PbSe well ($L_z$ = 3.5 nm) and the splitting between both peaks is already visible for the sample with larger wells ($L_z \geq$ 10.6 nm). In order to determine the strain inside the PbSe QW's, the (222) ω/2θ spectrum of the MQW samples was calculated in the framework of dynamical theory of X-ray diffraction, and compared to the measured ones. The perpendicular strain component $\varepsilon_{\perp}$ is obtained by Eq. 3 using elastic constants of the bulk material (Table 2), the calculated spectra that best fit to the measured data, using the in-plane lattice constant ($a_{||}$) as the main fitting parameter. The parallel strain ( $_{||}$) in the PbSe wells of each sample was then determined using this fitting procedure. Thus, it is also necessary to take into account the well width strain dependence.

The second strain source is thermal expansion differences between the semiconductor structure and the substrate (in our case $BaF_2$). An important question concerning IV-VI epitaxial structures grown on the $BaF_2$ substrates arises: Is there a temperature at which this thermal strain is zero? The experimental evidence (electrical and optical properties) indicates that the strain is practically zero at room temperature. The X-ray diffraction measurements show that thick epilayers are almost unstrained at 300 K (the total residual strain is lower than $3x10^{-4}$ for a thickness of 5 μm [15] or no strain to within $\pm 3x10^{-5}$ [16]). This result is important since our previous X-ray measurements gave only the lattice mismatch strain at room temperature.

There are two possible reasons for the negligible thermal strain near room temperature. On cooling the samples from their growth temperature a stress is generated at the interface and it is relieved by creation and movement of dislocations. In addition, although the thermal expansion coefficients (α) of IV-VI semiconductors and the $BaF_2$ substrate are similar they do

have a different temperature dependence: $\alpha$ (IV-VI) < $\alpha$ ($BaF_2$) at growth temperatures of $350^0$ C and $\alpha$ (IV-VI) > $\alpha$ ($BaF_2$) at temperatures less than ~ $100^0$ C. Thus, after sample cooling to room temperature, a partial compensation effect takes place.

On cooling the sample from room to cryogenic temperatures some residual elastic thermal strain in the sample is generated. This is based on a study [17] where this thermal strain in PbTe/$BaF_2$ films or PbTe/PbSnTe/$BaF_2$ superlattices was measured at low temperatures, and a value of $1.4x10^{-3}$ was obtained. The calculated thermal strain between PbTe and $BaF_2$ is $1.6x10^{-3}$, $1.4x10^{-3}$ and $0.88x10^{-3}$ at temperatures of 4 K, 30 K and 77 K, respectively. There is thus good agreement for a temperature of 30 K (the real sample temperature on the cold finger in the X-ray cryostat). These values both for PbTe and for PbSe should be added to the mismatched tensile strain values measured in the wells at room temperature.

## 4. Samples and optical measurements

The PbSe/PbSrSe [10] and PbTe/PbEuTe [9,14] MQW structures used are briefly described here. They were grown on freshly cleaved $BaF_2$ (111) substrates by MBE at temperatures of 360ºC and 300ºC, respectively. Before growing the MQW structure a thick (3-4 μm) buffer layer with the same composition as the barriers was grown in order to accommodate completely the lattice mismatch of 1% and 4.4% for PbSrSe/$BaF_2$ and PbEuTe/$BaF_2$, respectively. The barrier composition was chosen to get a barrier band gap of 0.5 eV or more at 300 K as verified from infrared absorption measurements. Therefore, the wells were deep enough at 300 K and $\Delta E_g$ increases at low temperatures. The well width was varied from 3 to 30 nm. The barrier thickness was varied from 40 to 50 nm. The number of periods was from 40 to 50.

The samples were characterized structurally by high resolution X-ray diffraction in the triple configuration to determine the barrier and well width lattice parameters [14]. Measurements were performed at room temperature. The strain in the wells inside the MQW structure was obtained as a function of its width using the common in-plane lattice constant as the main fitting parameter. It decreased monotonically with well width. MQW structures demonstrated a good resolved satellite peak structure that indicates their high quality (thickness reproducibility, homogeneous Eu or Sr content, and low interdiffusion).

Infrared transmission spectra were obtained at sample temperatures from 5 K to 300 K in a Fourier transform infrared spectrometer [9,10]. PL spectra were measured in pulsed mode at 4 K and 77 K using a Nd: YAG laser ($h\nu$ = 1.17 eV) for excitation and in CW mode at 300 K using an InGaAs laser ($h\nu$ = 1.28 eV) for the excitation. A gold-doped germanium (7.5 μm cutoff wavelength) or HgCdZnTe (6 μm cutoff wavelength) detector with a detectivity of $10^{10}$ cm·$Hz^{1/2}$/W was used. The energy resolution was 0.5-1 meV.

As-grown samples were used for the low temperature measurements. Emission lines in PL spectra are stimulated and they arise from the high energy side of spontaneous line, therefore, they represent with high accuracy the band gap. The differential absorption spectra of PbSe/PbSrSe MQW structures are obtained by taking the difference between a transmission spectrum at one temperature and the spectrum at a slightly lower temperature [10]. This takes advantage of the temperature dependence of the PbSe band gap, so that step edges associated with different transitions in the transmission spectra become peaks in the difference spectra. Thus the temperature difference spectra are in essence energy derivative spectra. Splitting of L-valley degeneracy and remarkable peak intensity difference were observed in the spectra. The last fact reflects the different densities of states in normal and

oblique valleys, i.e. transition intensity is much higher in the three-fold degenerate oblique valleys than in the one normal valley.

## 5. Results and discussion

As discussed above, depending mainly on the well width and on the specific values of the deformation potentials, the lowest optical transition in these QW structures can be either from the normal or from the oblique valleys. The corresponding transition energies are denoted by $E_{11}^N$ and $E_{11}^O$, respectively, and given by $E_{11}^{\nu} = E_g + \delta E_g{}^{\nu} + E_{e,1}{}^{\nu} + E_{h,1}{}^{\nu}$, where $\nu = N, O$ and $E_{(e,h),1}^{\nu}$ is the first electron or hole quantized state from the $\nu$ valley.

If we consider the pure strain effect for the [111] direction the following relation between the normal ($E_{11}^N$) and oblique valley ($E_{11}^O$) transition energies takes place: $E_{11}^N = E_{11}^O$ at $D_u = 0$; $E_{11}^N > E_{11}^O$ at $D_u < 0$; and $E_{11}^N < E_{11}^O$ at $D_u > 0$. The quantum-size effect increases both energies as the well width decreases. For example for PbSe, the $E_{11}^O$ energy is blue shifted twice as much as the $E_{11}^N$ energy due to anisotropy effects, i.e. the transverse effective mass is almost one half the longitudinal one. The final result of both energies depends on well width, effective mass, strain and deformation potential values.

In the first PL experiments [6] the relation $E_{11}^N < E_{11}^O$ was used for the PbTe well widths up to $L_z$ = 20 nm. Recent differential absorption spectroscopy results [10] clearly demonstrate that the following relation takes place also in PbSe: $E_{11}^N < E_{11}^O$ at well widths up to 30 nm. The evaluations at $L_z$ = 30 nm, where the level shifts due to quantum-size and deformation effects are comparable, show that the intervalley splitting $\Delta = E_{11}^N - E_{11}^O$ is relatively small. This means that $D_u$ is negative and that level crossing takes place due to the quantum size effect. Using $D_u$ = -0.2 eV we were able to get the calculated intervalley splitting very close to experimental values for three well widths at 4 K: 21.1, 7.3, and 3.8 meV for $L_z$ = 9.7, 20.6 and 29.7 nm, respectively. The well strain for each MQW structure was determined as discussed above. For the fitting we used the calculated $\Delta$ values for the $L_z$ = 20.6 nm and 29.7 nm. The large quantum-size contribution (~ 60 meV) at $L_z$ = 9.7 nm is less accurately given by the present two-band model. Imposing the $D_{iso}$ constraint, we thus obtain: $D_d$ = 5.3 eV and $D_u$ = -0.2 eV at 4 K.

With these deformation potentials, we have calculated the transition energies at 4 K as a function of the well width and, as shown in Figure, obtained very good agreement with the experimental data. To simplify the picture for each curve, we have used an averaged (over samples) fixed strain. In the case of 77 K, we have used the intervalley splitting $\Delta$ = 5.5 meV obtained at 66 K ($\varepsilon_{II} = 2.18 \times 10^{-3}$). The best fit here leads to $D_u$ = -0.5 eV and $D_d$ = 5.3 eV. Along with the PL data at 77 K, we have plotted also the absorption data at 66 K. They are near 5 meV lower than the theoretical curves due to the PbSe temperature gap coefficient (0.4 meV/K). The second PL line corresponding to $E_{22}^N$ transition was observed for sample $L_z$ = 10.6 nm at a high excitation level (~$10^5$ W/cm$^2$). Finally, the results at room temperature are plotted in the same Figure. Since the intervalley splitting (~10 meV) for $E_{11}$ transitions is small in comparison to kT at room temperature (26 meV) no differentiation between normal and oblique valleys is observed; most of the experimental points lay between the calculated curves.

Thus good agreement was obtained between the low energy state differential spectroscopy and PL data, on the one hand, and the calculations in the framework of the two-band model, which is also valid for the low energy states, on the other hand.

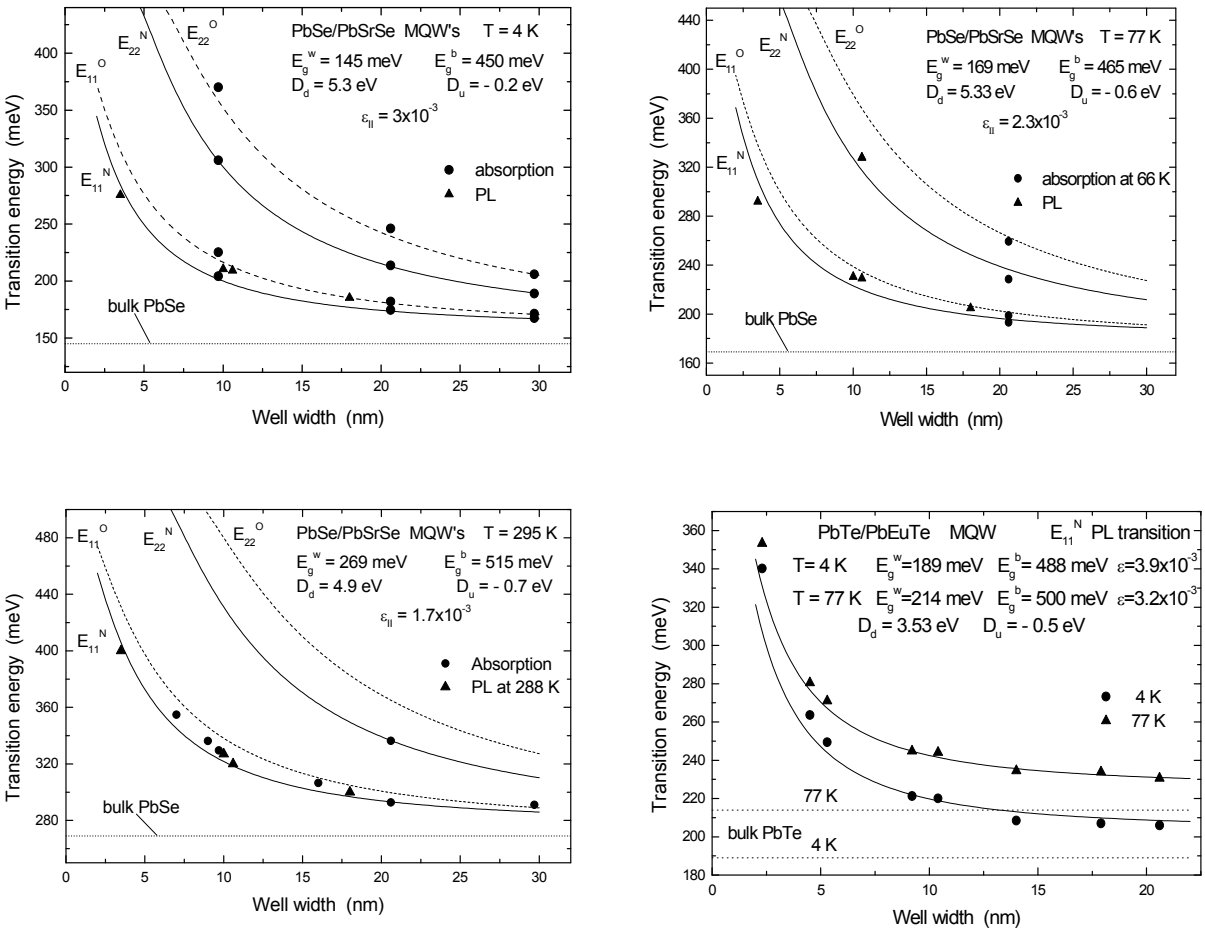


Figure. Calculated sub-band transition energies versus well width for PbSe/PbSrSe MQWs at 4, 77 and 295 K, and for PbTe/PbEuTe MQWs at 4 and 77 K. The solid and dashed lines correspond to transitions in normal (longitudinal) and oblique valleys, respectively. The total strain $\varepsilon_{II}$ is averaged over samples for each curve.

It should be noted that the PbSe deformation potential values change with temperature: $D_d$ slightly decreases and $D_u$ by several times increases with increasing temperature (see Table 1). Taking into account that $D_d$ and $D_u$ are differences of big quantities we can conclude that the acoustic potential values change with temperature.

The PbTe optical deformation potential constants were obtained (see below) from laser [18] and magneto-optical [5,19] measurements of PbTe/$BaF_2$ structures at low temperatures and they are: $D_d$ = 3.53 eV and $D_u$ = -0.5 eV. We have used these values for calculation of quantum well transition energies, which are compared with photoluminescence data for PbTe/PbEuTe MQW structures. Considering the previous evaluations of the thermal strain ($\varepsilon_{II} = 1.6\text{x}10^{-3}$ at 4 K and $\varepsilon_{II} = 0.9\text{x}10^{-3}$ at 77 K) and of the measured [14] mismatch strain (which depends on the well width and changes from $1.9\text{x}10^{-3}$ and $2.7\text{x}10^{-3}$), we have used an averaged total strain of $\varepsilon_{II} = 3.9\text{x}10^{-3}$ and $3.2\text{x}10^{-3}$ at 4 K and 77 K, respectively. Calculations

of the lowest (normal valley) transition energy at two temperatures are shown in the Figure where the photoluminescence data points are also presented.

As one can see in the Figure, some deviations between experimental and calculated transition energy values take place in the narrowest quantum wells ($L_z$ = 2.3 and 3.5 nm for the PbTe/PbEuTe and PbSe/PbSrSe MQW's, respectively) due to the decreasing accuracy of the two-band model with increasing energy. For these high energy transitions the six-band model should be used. It should be also noted that the obtained optical deformation potential constants for PbTe differ from most of the available data in the literature [1,6], except for the $D_u$ value proposed in [4,5]. For more detail discussions of deformation energy shifts observed in different publications see in [20].

Summarizing, with the use of measured strain induced intervalley splitting energies, empirical isotropic deformation potentials, and a detailed analysis of the strain we were able to determine new optical deformation potential values for PbSe and PbTe. At 4 K, for example, we have found: $D_u$ = -0.2 and -0.5 eV, and $D_d$ = 5.3 and 3.5 eV for PbSe and PbTe, respectively. They result from the best fit to the photoluminescence and differential absorption spectroscopy data using an envelope function calculation based on an accurate two-band **k·p** model for the bulk. In general, but more specifically at low temperatures, a small uniaxial optical deformation potential constant ($D_u$) is obtained for both PbSe and PbTe due probably to the mirror symmetry of the conduction and valence bands in these materials.

## References


[1] L. G. Ferreira, Phys. Rev. **137A**, 1601 (1965).
[2] Rabii Sohrab, Phys. Rev. **167**, 801 (1968).
[3] P. Enders, Phys. Stat. Sol. (b), **129**, 89; **132**, 165 (1985).
[4] M. Kriechbaum, K. E. Ambrosch, E. F. Fantner, H. Pascher, H. Clemens, and G. Bauer, Phys. Rev. **30**, 3394 (1984).
[5] J. Singleton, E. Kress-Rogers, A. V. Lewis, R. J. Nicholas, E. J. Fantner, G. Bauer, and A. Lopez-Otero, J. Phys. C: Solid State Phys. **19**, 77 (1986).
[6] M. V. Valeiko, I. I. Zasavitskii, A. V. Matveenko, B. N. Matsonashvili, and Z.A. Rukhadze, Superlattices and Microstructures **9**, 195 (1991).
[7] H. Wu, N. Dai, and P. J. McCann, Phys. Rev. B **66**, 045303 (2002).
[8] M. Schlüter, G. Martinez, and M. L. Cohen, Phys. Rev. B **12**, 650 (1975).
[9] E. Abramof, E. A. de Andrada e Silva, S. O. Ferreira, P. Motisuke, P. H. O. Rappl, and A.Y. Ueta, Phys. Rev. B **63**, 085304 (2001).
[10] H. Z. Wu, N. Dai, M. B. Johnson, P. J. McCann, and Z. S. Shi, Appl. Phys. Lett. **78**, 2199, (2001).
[11] B. Houston, R. E. Strakna, and H. S. Belson, J. Appl. Phys. **39**, 3913 (1968).
[12] G. Lippmann, P. Kästner, and W. Wanninger, Phys. Stat. Sol. (a), **6**, K159 (1971).
[13] E. A. de Andrada e Silva, Phys. Rev. B **60**, 8859 (1999).
[14] E. Abramof, P. H. O. Rappl, A. Y. Ueta, and P. Motisuke, J. Appl. Phys. **88**, 725 (2000).
[15] E. J. Fantner, B. Ortner, W. Ruhs, and A. Lopez-Otero, *Lecture Notes in Physics*, ed. by E. Gornik, H. Heinrich, and L. Palmetshofer (Springer-Verlag, Berlin, Heidelberg, New York, 1982), Vol. 152, p. 59.
[16] D. K. Hohnke and M. D. Hurley, J. Appl. Phys. **47**, 4975 (1976).
[17] E. J. Fantner, Appl. Phys. Lett. **47**, 803 (1985).
[18] W. H. Weber and K. F. Yeung, J. Appl. Phys. **44**, 4991 (1973).
[19] J. Oswald, P. Pichler, B. B. Goldberg, and G. Bauer, Phys. Rev. B **49**, 17029 (1994).
[20] I. I. Zasavitskii, E. A. de Andrada e Silva, E. Abramof, P. J. McCann, Phys. Rev. B **70**, 115302 (2004).